# Supporting Information for

# Lattice Engineering to Simultaneously Control the Defect/Stacking Structures of Layered Double Hydroxide Nanosheets to Optimize Their Energy Functionalities

*Najin Kim,*[†,▽] *Tae-Ha Gu,*[†,▽] *Dongyup Shin,*[‡,▽] *Xiaoyan Jin,*[#] *Hyeyoung Shin,*[§] *Min Gyu Kim,*[¶]

*Hyungjun Kim,*[‡,*] *and Seong-Ju Hwang*[#,*]

[†] Department of Chemistry and Nanoscience, Ewha Womans University, Seoul 03760, Republic of Korea

[‡] Department of Chemistry, Korea Advanced Institute of Science and Technology (KAIST), Daejeon 34141, Republic of Korea

[#] Department of Materials Science and Engineering, Yonsei University, Seoul 03722, Republic of Korea

[§] Graduate School of Energy Science and Technology (GEST), Chungnam National University, Daejeon 34134, Republic of Korea

[¶] Beamline Research Division, Pohang Accelerator Laboratory (PAL), Pohang 37673, Republic of Korea

**Corresponding Author:** *linus16@kaist.ac.kr (H.K.); *hwangsju@yonsei.ac.kr (S.-J.H.).

**Table S1.** Ionic radii and hydration shell radii of various anions.

| | $Cl^-$ | $Br^-$ | $I^-$ | $NO_3^-$ |
|---|---|---|---|---|
| Ionic radius (nm) | 0.181 | 0.196 | 0.220 | 0.244 |
| Hydration shell radius (nm) | 0.224 | 0.231 | 0.246 | 0.288 |

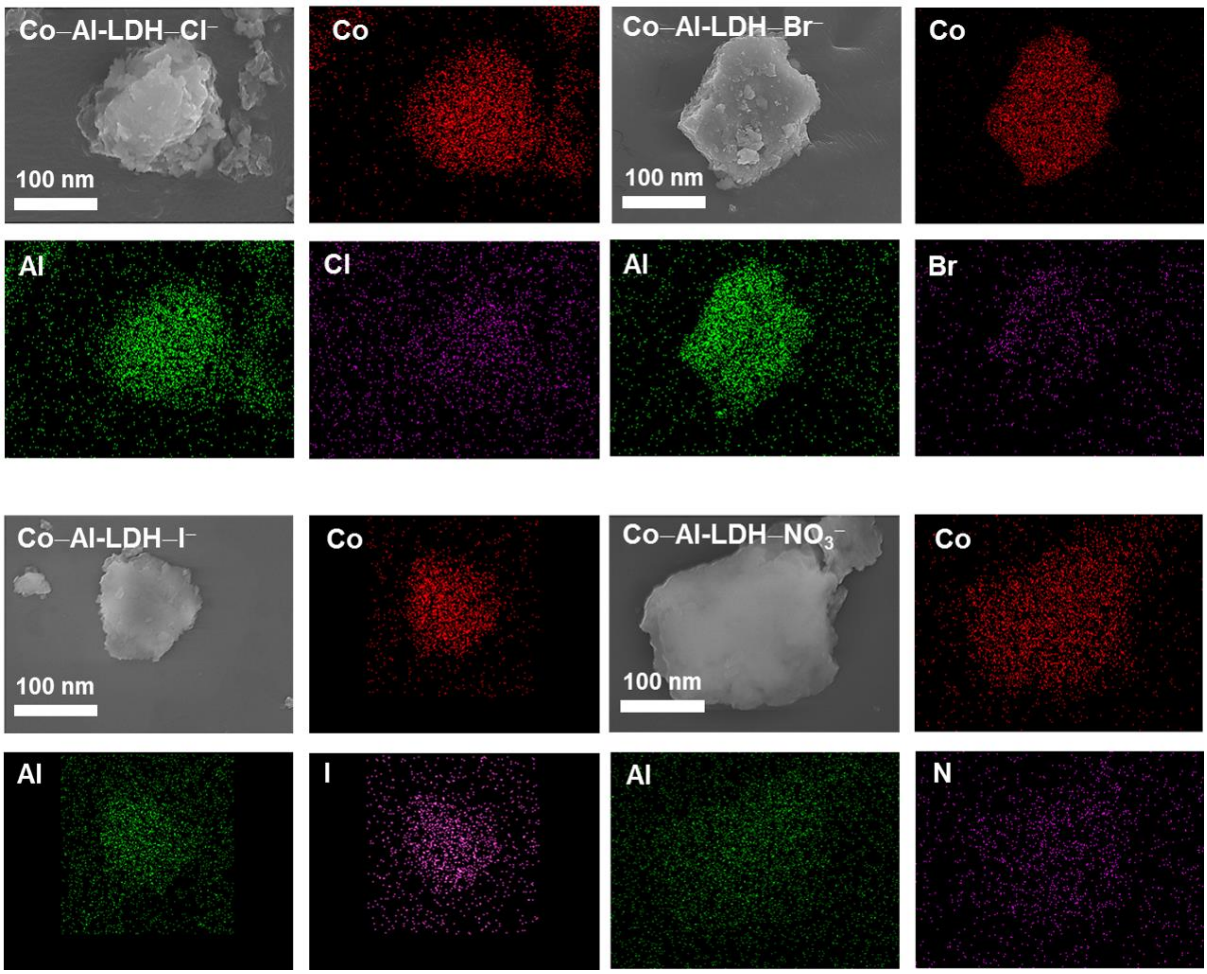


**Figure S1.** Energy dispersive spectrometry (EDS)–elemental maps of restacked Co–Al-layered double hydroxide (LDH) nanosheets (NSs).

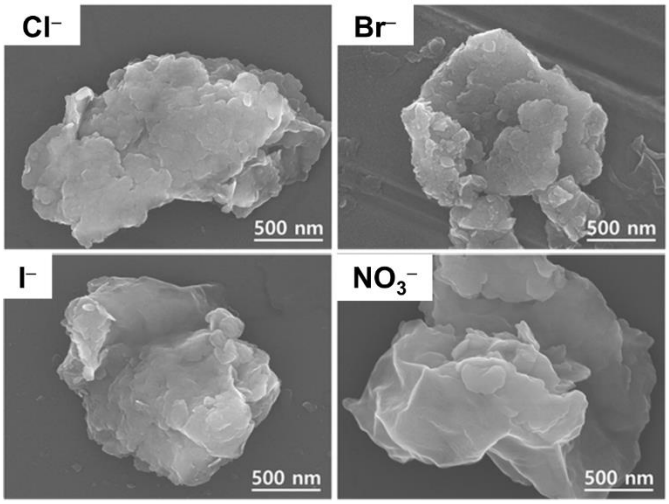


**Figure S2.** The field emission-scanning electron microscopy (FE-SEM) images of restacked Co–Al-LDH NSs.

**Table S2.** Results of non-linear least-squares curves-fittings for the Co K-edge extended X-ray absorption fine structure (EXAFS) spectra of restacked Co–Al-LDH NSs.

| Material | Bond | Coordination number (CN) | R (Å) | Debye–Waller ($\sigma^2$) ($10^{-3} \times Å^2$) |
|---|---|---|---|---|
| Co–Al-LDH–$Cl^-$ | Co–O | 5.78 | 2.07 | 4.62 |
| | Co–Al | 1.43 | 2.99 | 6.68 |
| | Co–Co | 2.86 | 3.15 | 6.68 |
| Co–Al-LDH–$Br^-$ | Co–O | 5.59 | 2.08 | 5.55 |
| | Co–Al | 1.28 | 3.00 | 7.51 |
| | Co–Co | 2.56 | 3.16 | 7.51 |
| Co–Al-LDH–$I^-$ | Co–O | 5.35 | 2.08 | 6.43 |
| | Co–Al | 1.26 | 3.00 | 7.83 |
| | Co–Co | 2.52 | 3.16 | 7.83 |
| Co–Al-LDH–$NO_3^-$ | Co–O | 5.24 | 2.08 | 7.27 |
| | Co–Al | 1.02 | 3.00 | 8.36 |
| | Co–Co | 2.04 | 3.16 | 8.36 |

**Table S3.** The chemical compositions and oxygen vacancy contents of restacked Co−Al-LDH NSs.

| Material | Chemical composition | Oxygen vacancy content (%) |
|---|---|---|
| Co−Al-LDH−$Cl^-$ | $[Co_{0.58}Al_{0.35}(OH)_{1.92}]Cl_{0.70}$ | 4.0 |
| Co−Al-LDH−$Br^-$ | $[Co_{0.60}Al_{0.38}(OH)_{1.88}]Br_{0.73}$ | 6.0 |
| Co−Al-LDH−$I^-$ | $[Co_{0.62}Al_{0.38}(OH)_{1.83}]I_{0.76}$ | 8.5 |
| Co−Al-LDH−$NO_3^-$ | $[Co_{0.63}Al_{0.37}(OH)_{1.78}](NO_3)_{0.76}$ | 11.0 |

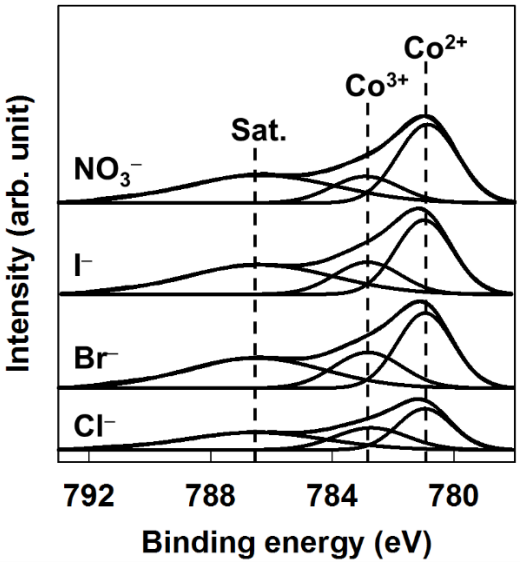


**Figure S3.** Co $2p_{3/2}$ X-ray photoelectron spectroscopy (XPS) data for restacked Co–Al-LDH NSs.

**Table S4.** Relative concentrations of $Co^{2+}$ and $Co^{3+}$ ions for restacked Co–Al-LDH NSs.

| Material | $Co^{2+}/Co^{3+}$ ratio |
|---|---|
| Co–Al-LDH–$Cl^-$ | 1.403 |
| Co–Al-LDH–$Br^-$ | 1.724 |
| Co–Al-LDH–$I^-$ | 1.985 |
| Co–Al-LDH–$NO_3^-$ | 2.635 |

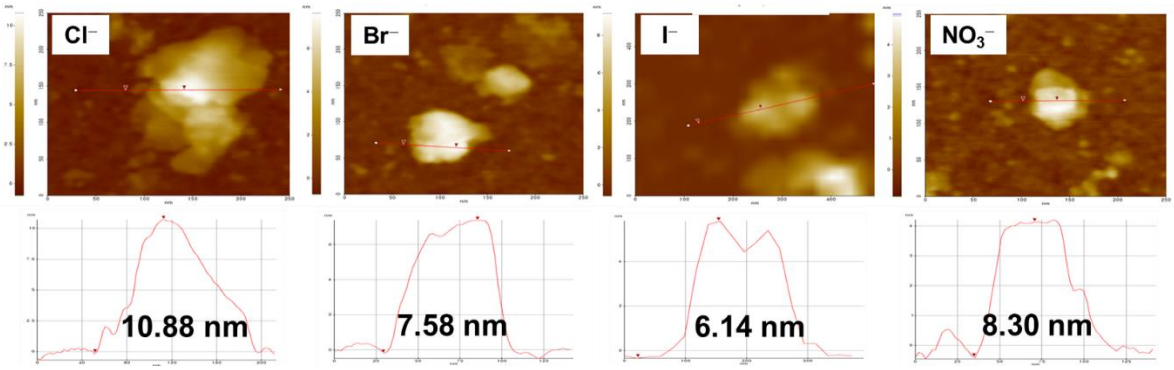


**Figure S4.** Atomic force microscopy (AFM) images of restacked Co−Al-LDH NSs.

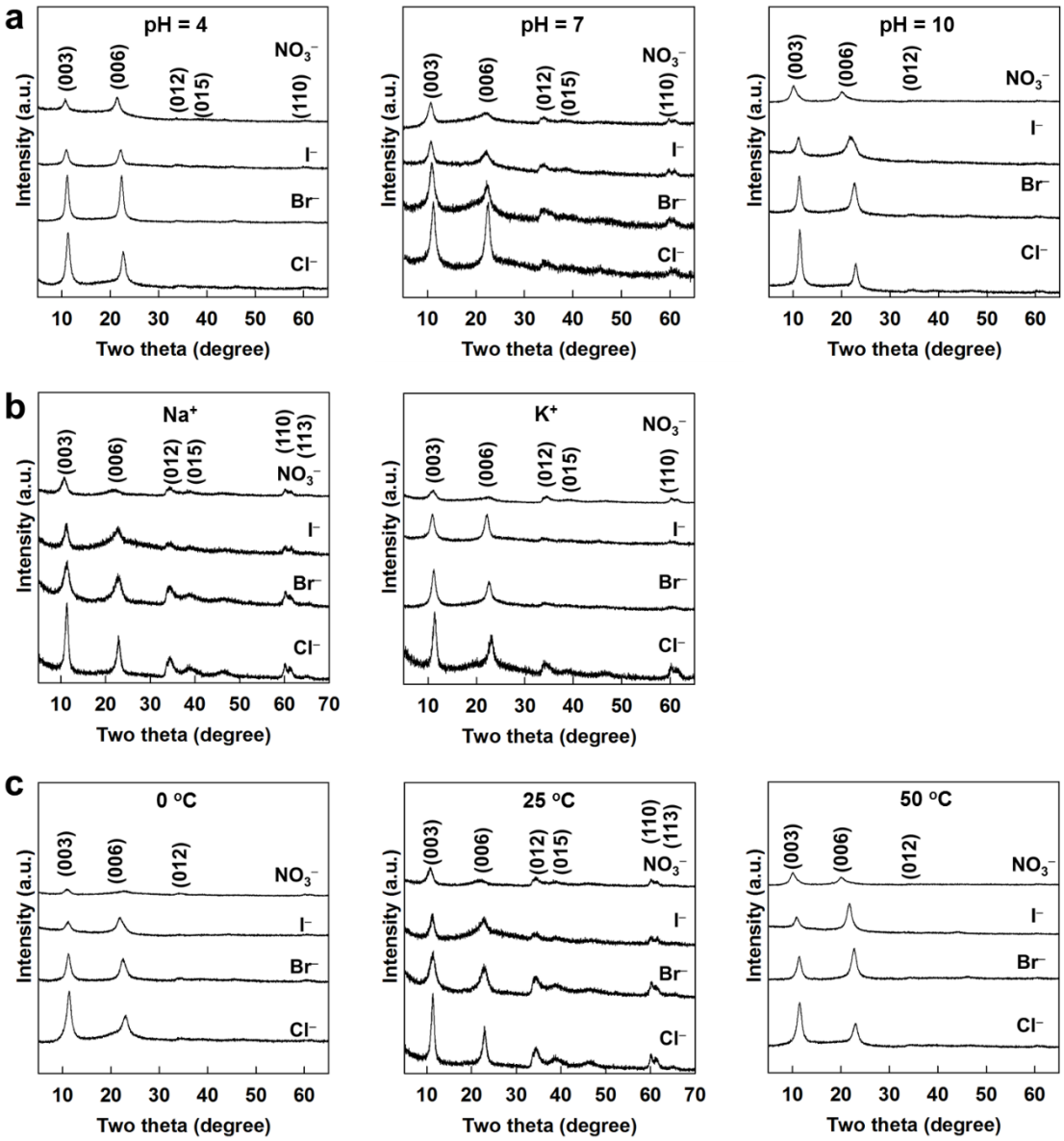


**Figure S5.** Powder X-ray diffraction (XRD) data of restacked Co–Al-LDH NSs synthesized with (a) pH change, (b) cation change, and (c) temperature change.

**Table S5.** Stacking structures for restacked Co−Al-LDH NSs synthesized with the pH change, cation change, and temperature change.

| Condition | Material | Interlayer spacing (Å) | Layer thickness (nm) | Stacking number |
|---|---|---|---|---|
| pH = 4 | Co−Al-LDH−$Cl^-$ | 7.79 | 8.7 | 11.2 |
| pH = 4 | Co−Al-LDH−$Br^-$ | 7.93 | 7.0 | 8.8 |
| pH = 4 | Co−Al-LDH−$I^-$ | 8.03 | 5.6 | 7.0 |
| pH = 4 | Co−Al-LDH−$NO_3^-$ | 8.15 | 5.1 | 6.3 |
| pH = 7 | Co−Al-LDH−$Cl^-$ | 7.80 | 9.2 | 11.8 |
| pH = 7 | Co−Al-LDH−$Br^-$ | 8.01 | 6.3 | 7.9 |
| pH = 7 | Co−Al-LDH−$I^-$ | 8.12 | 5.1 | 6.3 |
| pH = 7 | Co−Al-LDH−$NO_3^-$ | 8.22 | 4.1 | 4.9 |
| pH = 10 | Co−Al-LDH−$Cl^-$ | 7.71 | 8.7 | 11.3 |
| pH = 10 | Co−Al-LDH−$Br^-$ | 7.78 | 7.9 | 10.2 |
| pH = 10 | Co−Al-LDH−$I^-$ | 7.89 | 7.1 | 9.0 |
| pH = 10 | Co−Al-LDH−$NO_3^-$ | 8.62 | 4.6 | 5.3 |
| $Na^+$, 25 °C | Co−Al-LDH−$Cl^-$ | 7.81 | 10.5 | 13.5 |
| $Na^+$, 25 °C | Co−Al-LDH−$Br^-$ | 7.87 | 7.8 | 9.9 |
| $Na^+$, 25 °C | Co−Al-LDH−$I^-$ | 8.00 | 6.5 | 8.1 |
| $Na^+$, 25 °C | Co−Al-LDH−$NO_3^-$ | 8.15 | 4.6 | 5.6 |
| $K^+$ | Co−Al-LDH−$Cl^-$ | 7.80 | 9.5 | 12.2 |
| $K^+$ | Co−Al-LDH−$Br^-$ | 7.88 | 7.4 | 9.4 |
| $K^+$ | Co−Al-LDH−$I^-$ | 8.01 | 6.9 | 8.6 |
| $K^+$ | Co−Al-LDH−$NO_3^-$ | 8.06 | 4.5 | 5.6 |
| 0 °C | Co−Al-LDH−$Cl^-$ | 7.73 | 7.2 | 9.3 |
| 0 °C | Co−Al-LDH−$Br^-$ | 7.83 | 6.4 | 8.2 |

| | | | | |
|---|---|---|---|---|
| 0 °C | Co–Al-LDH–$I^-$ | 7.87 | 5.8 | 7.4 |
| 0 °C | Co–Al-LDH–$NO_3^-$ | 8.00 | 4.4 | 5.5 |
| 50 °C | Co–Al-LDH–$Cl^-$ | 7.70 | 7.8 | 10.1 |
| 50 °C | Co–Al-LDH–$Br^-$ | 7.74 | 7.4 | 9.6 |
| 50 °C | Co–Al-LDH–$I^-$ | 8.15 | 7.1 | 8.7 |
| 50 °C | Co–Al-LDH–$NO_3^-$ | 8.72 | 5.6 | 6.4 |

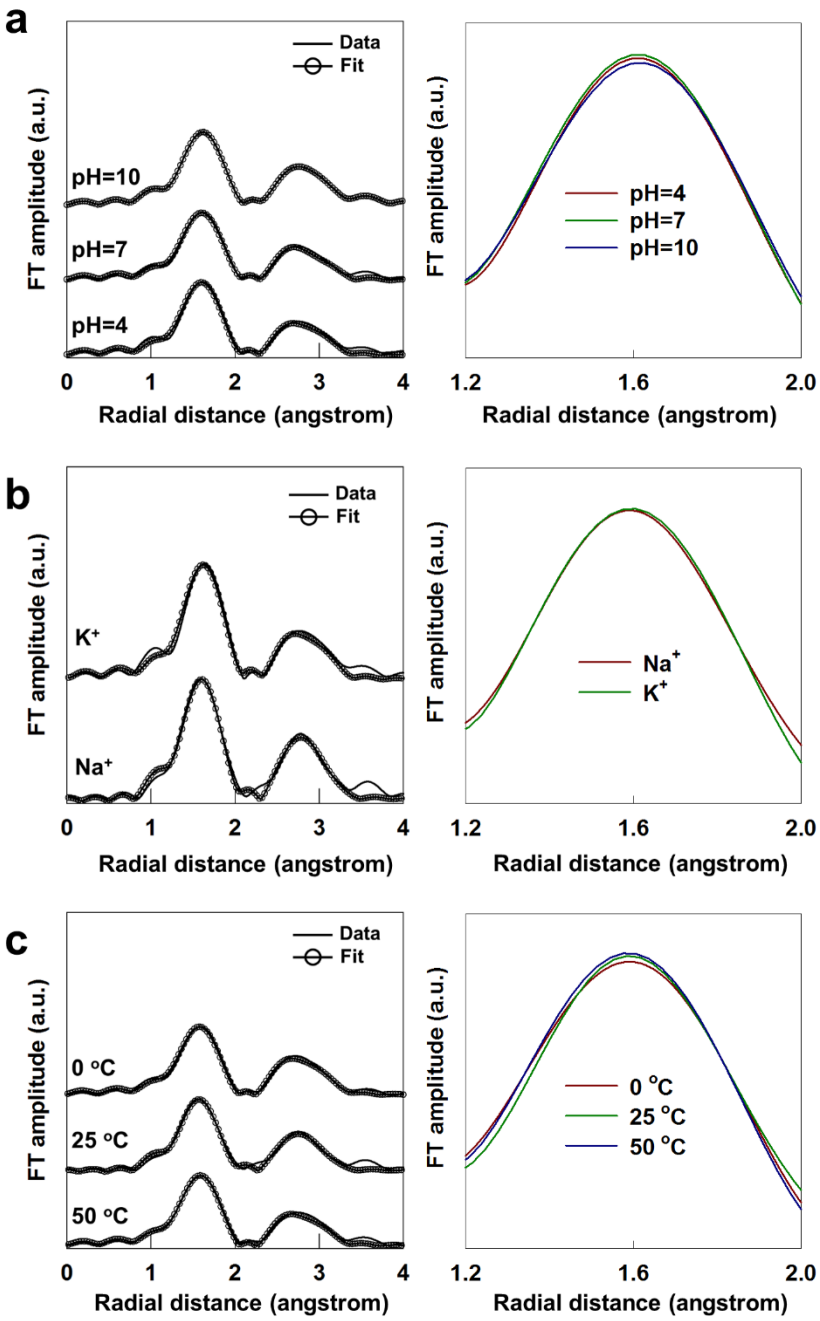


**Figure S6.** Fourier transforms (FTs) of Co K-edge EXAFS of Co–Al-LDH–$NO_3^-$ synthesized with (a) pH change, (b) cation change, and (c) temperature change.

**Table S6.** Results of Co K-edge EXAFS fitting analysis for Co–Al-LDH–$NO_3^-$ synthesized with the pH change, cation change, and temperature change.

| Condition | Bond | CN | R (Å) | $\sigma^2$ ($10^{-3} \times$ Å$^2$) |
|---|---|---|---|---|
| pH = 4 | Co–O | 5.27 | 2.08 | 7.34 |
| | Co–Al | 1.04 | 2.99 | 7.82 |
| | Co–Co | 2.05 | 3.15 | 7.82 |
| pH = 7 | Co–O | 5.27 | 2.08 | 7.17 |
| | Co–Al | 1.05 | 2.99 | 8.25 |
| | Co–Co | 2.05 | 3.15 | 8.25 |
| pH = 10 | Co–O | 5.25 | 2.08 | 7.84 |
| | Co–Al | 1.04 | 2.99 | 8.45 |
| | Co–Co | 2.04 | 3.15 | 8.45 |
| $Na^+$, 25 °C | Co–O | 5.24 | 2.08 | 7.45 |
| | Co–Al | 1.02 | 2.99 | 8.64 |
| | Co–Co | 2.04 | 3.15 | 8.64 |
| $K^+$ | Co–O | 5.24 | 2.08 | 7.74 |
| | Co–Al | 1.01 | 2.99 | 9.59 |
| | Co–Co | 2.02 | 3.15 | 9.59 |
| 0 °C | Co–O | 5.23 | 2.08 | 7.86 |
| | Co–Al | 1.05 | 2.99 | 8.28 |
| | Co–Co | 2.06 | 3.15 | 8.28 |
| 50 °C | Co–O | 5.24 | 2.08 | 7.56 |
| | Co–Al | 1.02 | 2.99 | 8.87 |
| | Co–Co | 2.03 | 3.15 | 8.87 |

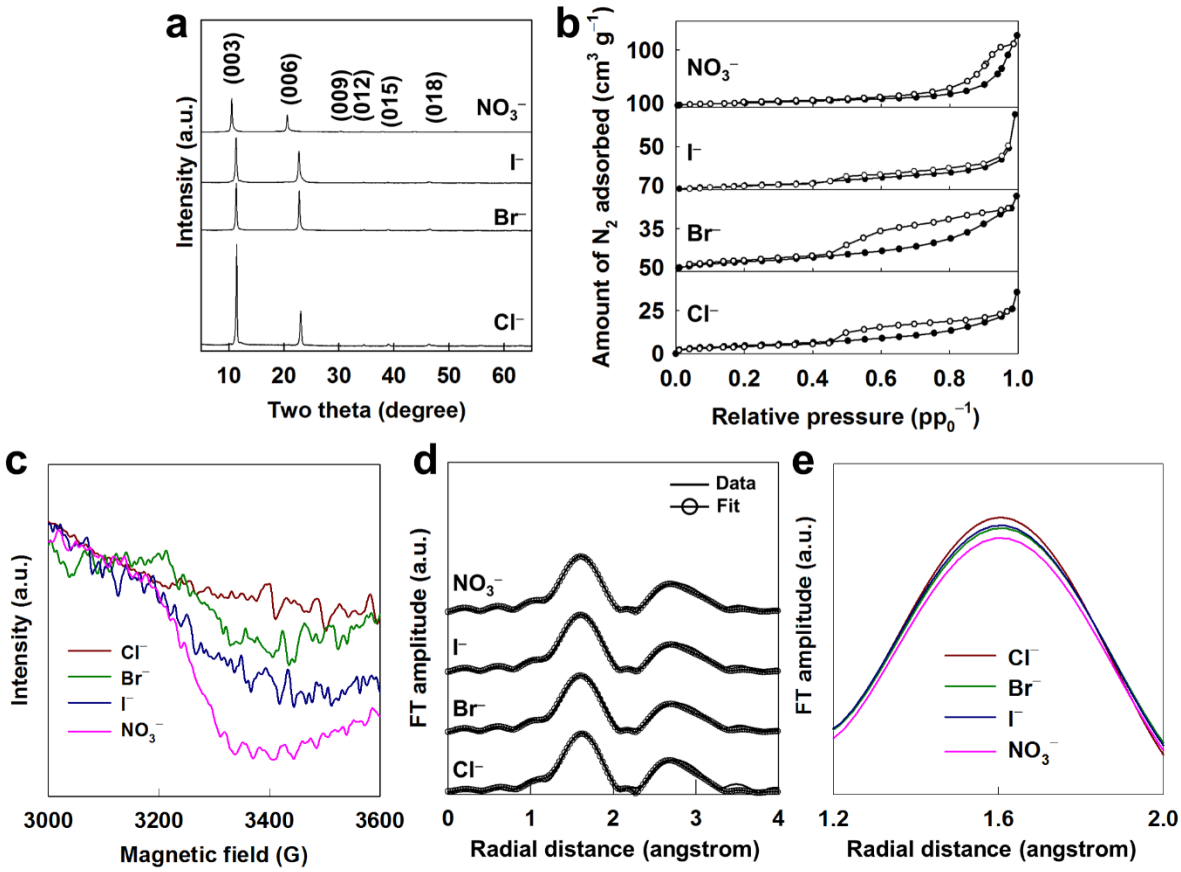


**Figure S7.** (a) Powder XRD, (b) $N_2$ adsorption–desorption isotherm data, (c) electron paramagnetic resonance (EPR) spectra, and (d, e) FTs of Co K-edge EXAFS data of ion-exchanged Co–Al-LDH materials.

**Table S7.** Stacking structures, pore structures, and Co K-edge EXAFS fitting results for ion-exchanged Co–Al-LDH materials.

| Material | Interlayer spacing (Å) | Layer thickness (nm) | Stacking number | Surface area ($m^2\ g^{-1}$) | Pore volume ($cm^3\ g^{-1}$) |
|---|---|---|---|---|---|
| Co–Al-LDH–$Cl^-$ | 7.69 | 28.6 | 37.2 | 17 | 0.09 |
| Co–Al-LDH–$Br^-$ | 7.75 | 25.0 | 32.3 | 25 | 0.13 |
| Co–Al-LDH–$I^-$ | 7.80 | 23.5 | 30.1 | 33 | 0.18 |
| Co–Al-LDH–$NO_3^-$ | 8.36 | 21.0 | 25.1 | 50 | 0.30 |

| Material | Bond | CN | R (Å) | $\sigma^2$ ($10^{-3} \times Å^2$) |
|---|---|---|---|---|
| Co–Al-LDH–$Cl^-$ | Co–O | 5.91 | 2.08 | 2.66 |
| | Co–Al | 1.60 | 2.97 | 3.57 |
| | Co–Co | 3.20 | 3.13 | 3.57 |
| Co–Al-LDH–$Br^-$ | Co–O | 5.86 | 2.08 | 4.61 |
| | Co–Al | 1.51 | 2.97 | 5.32 |
| | Co–Co | 3.02 | 3.13 | 5.32 |
| Co–Al-LDH–$I^-$ | Co–O | 5.78 | 2.08 | 4.94 |
| | Co–Al | 1.39 | 2.97 | 6.87 |
| | Co–Co | 2.78 | 3.13 | 6.87 |
| Co–Al-LDH–$NO_3^-$ | Co–O | 5.60 | 2.08 | 7.34 |
| | Co–Al | 1.31 | 2.97 | 8.21 |
| | Co–Co | 2.62 | 3.13 | 8.21 |

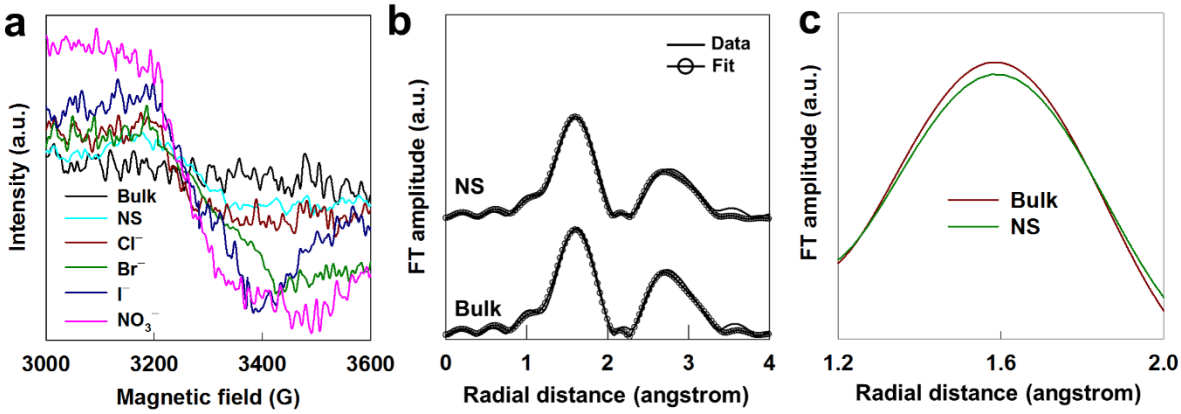


**Figure S8.** (a) EPR spectra and (b, c) FTs of Co K-edge EXAFS data of bulk Co–Al-LDH, exfoliated Co–Al-LDH NS, and restacked Co–Al-LDH NSs.

**Table S8.** Results of Co K-edge EXAFS fitting analysis for bulk Co−Al-LDH and exfoliated Co−Al-LDH NS.

| Material | Bond | CN | R (Å) | $\sigma^2$ ($10^{-3} \times Å^2$) |
|---|---|---|---|---|
| Bulk Co−Al-LDH | Co−O | 6.00 | 2.06 | 1.27 |
| | Co−Al | 1.95 | 2.97 | 2.05 |
| | Co−Co | 3.89 | 3.13 | 2.05 |
| Co−Al-LDH NS | Co−O | 5.83 | 2.06 | 3.14 |
| | Co−Al | 1.77 | 2.97 | 4.66 |
| | Co−Co | 3.54 | 3.13 | 4.66 |

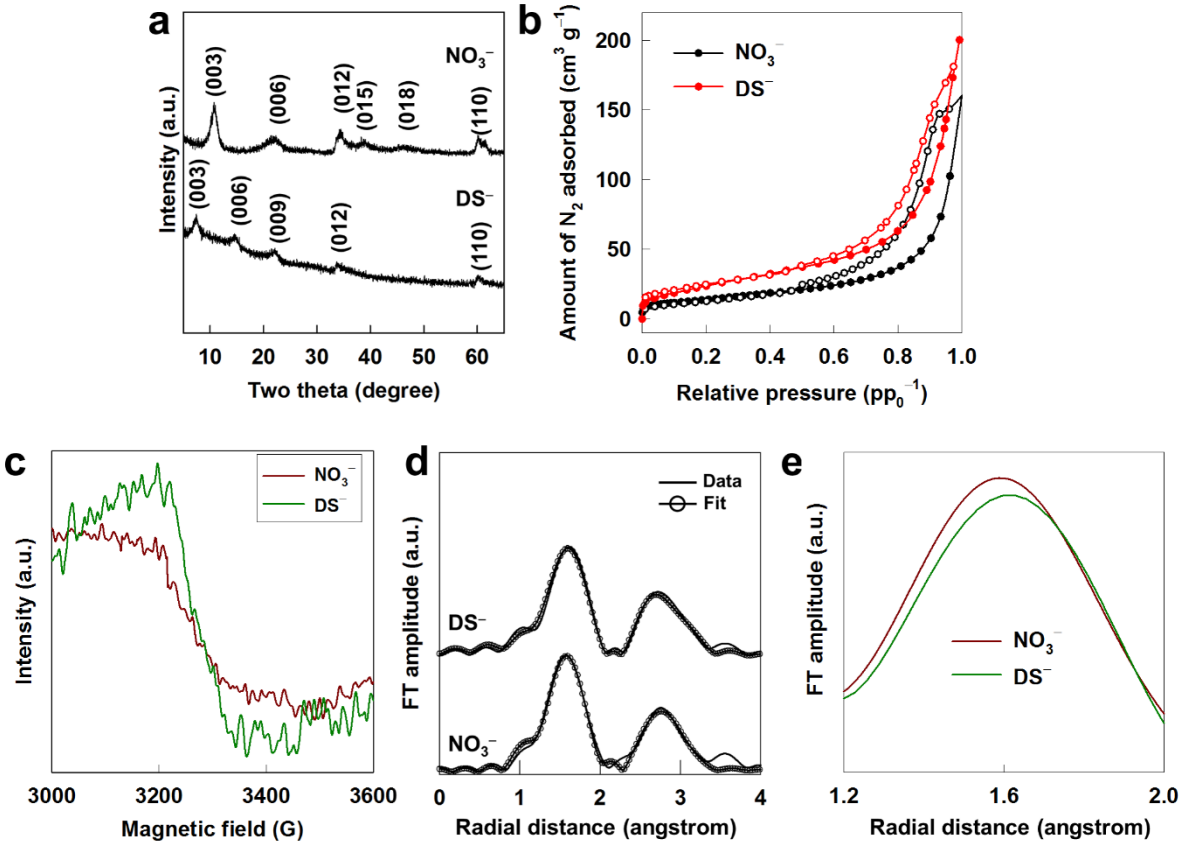


**Figure S9.** (a) Powder XRD, (b) $N_2$ adsorption–desorption isotherm data, (c) EPR spectra, and (d, e) FTs of Co K-edge EXAFS data of Co–Al-LDH–$DS^-$ and Co–Al-LDH–$NO_3^-$.

**Table S9.** Stacking structures, pore structures, and Co K-edge EXAFS fitting results for Co–Al-LDH–$DS^-$ and Co–Al-LDH–$NO_3^-$.

| Material | Interlayer spacing (Å) | Layer thickness (nm) | Stacking number | Surface area ($m^2\ g^{-1}$) | Pore volume ($cm^3\ g^{-1}$) |
|---|---|---|---|---|---|
| Co–Al-LDH–$NO_3^-$ | 8.15 | 4.6 | 5.6 | 89 | 0.61 |
| Co–Al-LDH–$DS^-$ | 11.26 | 4.2 | 3.7 | 104 | 0.77 |

| Material | Bond | CN | R (Å) | $\sigma^2$ ($10^{-3} \times Å^2$) |
|---|---|---|---|---|
| Co–Al-LDH–$NO_3^-$ | Co–O | 5.24 | 2.08 | 7.45 |
| | Co–Al | 1.02 | 2.99 | 8.64 |
| | Co–Co | 2.04 | 3.15 | 8.64 |
| Co–Al-LDH–$DS^-$ | Co–O | 5.12 | 2.10 | 9.17 |
| | Co–Al | 1.02 | 3.00 | 10.5 |
| | Co–Co | 2.05 | 3.16 | 10.5 |

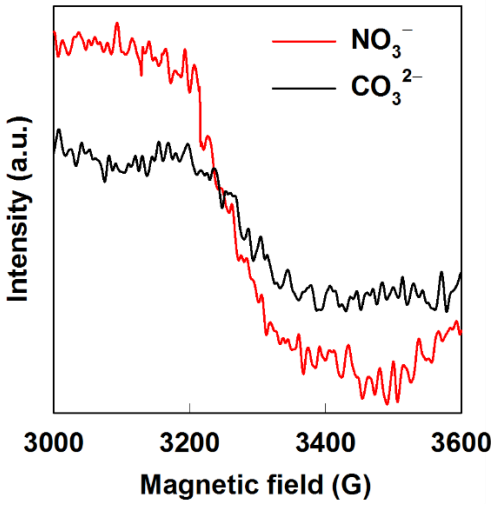


**Figure S10.** (a) EPR spectra of Co–Al-LDH–$CO_3^{2-}$ and Co–Al-LDH–$NO_3^-$.

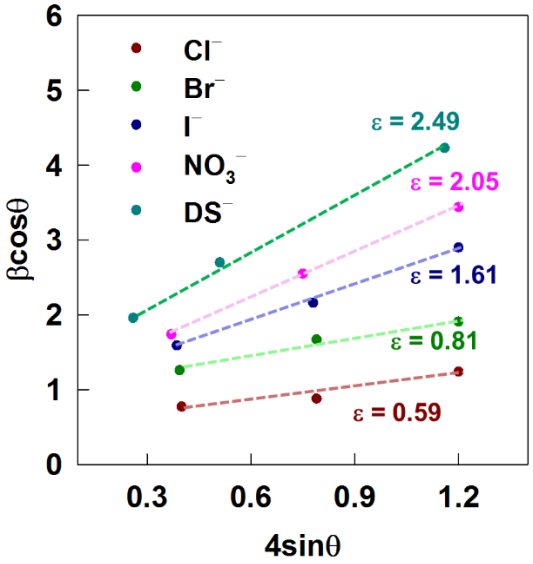


**Figure S11.** Lattice strains of restacked Co–Al-LDH NSs.

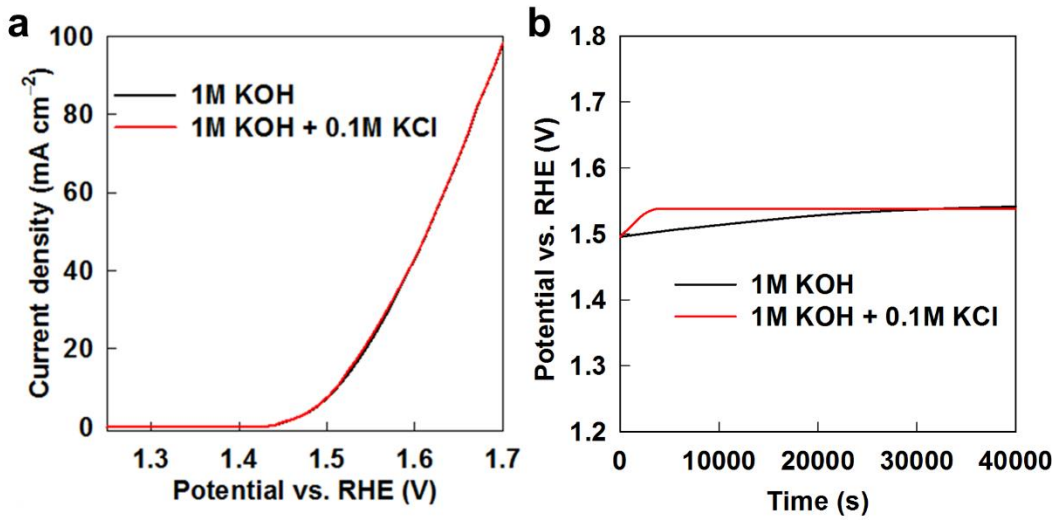


**Figure S12.** (a) Linear sweep voltammetry (LSV) curves and (b) stability tests for Co–Al-LDH–$NO_3^-$ with/without $Cl^-$ ions in electrolyte.

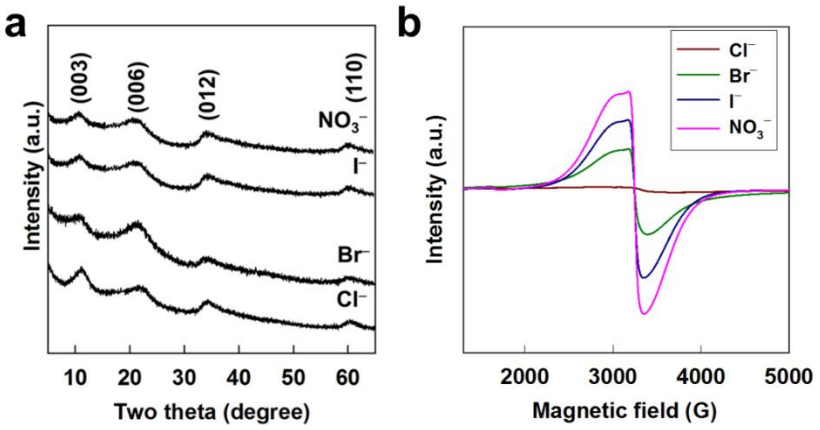


**Figure S13.** (a) Powder XRD and (b) EPR spectra of restacked Ni–Fe-LDH NSs.

**Table S10.** Stacking structures of restacked Ni–Fe-LDH NSs.

| Material | Interlayer spacing (Å) | Layer thickness (nm) | Stacking number |
|---|---|---|---|
| Ni–Fe-LDH–$Cl^-$ | 7.86 | 4.3 | 5.2 |
| Ni–Fe-LDH–$Br^-$ | 8.10 | 4.2 | 5.1 |
| Ni–Fe-LDH–$I^-$ | 8.21 | 4.0 | 5.0 |
| Ni–Fe-LDH–$NO_3^-$ | 8.28 | 3.8 | 4.9 |

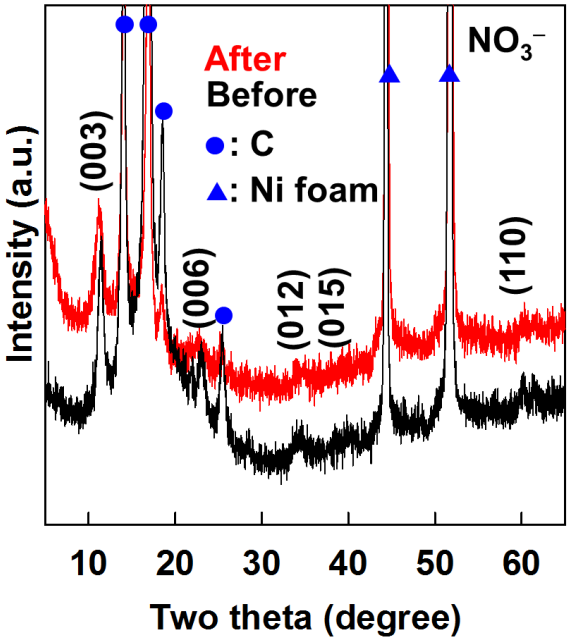


**Figure S14.** Powder XRD data of Co–Al-LDH–$NO_3^-$ after OER stability test. For the XRD measurement, the nickel foam was adopted as the electrode instead of glassy carbon, because the amount of catalyst supported on glassy carbon was too small for XRD analysis.

**Table S11.** Specific capacitances of carbon-free LDH-based electrode materials.

| Material composition | Specific capacitance / Current density, Scan rate | Ref. |
|---|---|---|
| Co–Al-LDH–dodecyl sulfate | 1482 F $g^{-1}$ / 1 A $g^{-1}$ | 1 |
| Co–Al LDH/$Ni(OH)_2$ | 1811 F $g^{-1}$ / 2 A $g^{-1}$ | 2 |
| Co–Al-LDH–OH | 1031 F $g^{-1}$ / 1 A $g^{-1}$ | 3 |
| $Co(OH)_2$@Co–Al-LDH | 1734 F $g^{-1}$ / 5 mA $cm^{-2}$ | 4 |
| Porous Co–Al-LDH flower | 550 F $g^{-1}$ / 10 A $g^{-1}$ | 5 |
| 3D Co–Al-LDH | 838 F $g^{-1}$ / 1 A $g^{-1}$ | 6 |
| Co–Al-LDH@$Ni(OH)_2$ nanosheet array | 1528 F $g^{-1}$/ 5 mA $cm^{-2}$ | 7 |
| NiP@Co–Al-LDH | 556 C $g^{-1}$ / 1 mA $cm^{-2}$ | 8 |

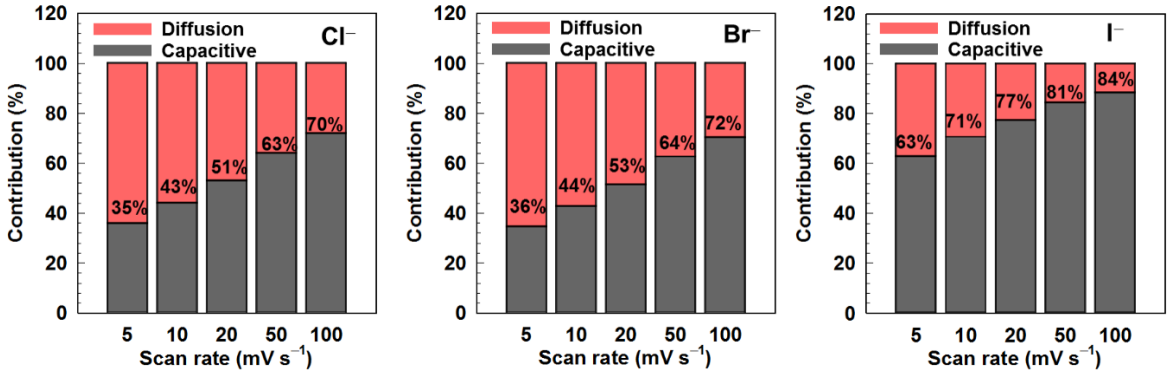


**Figure S15.** The fractions of the capacitive and diffusion-controlled contributions of restacked Co−Al-LDH NSs at various scan rates.

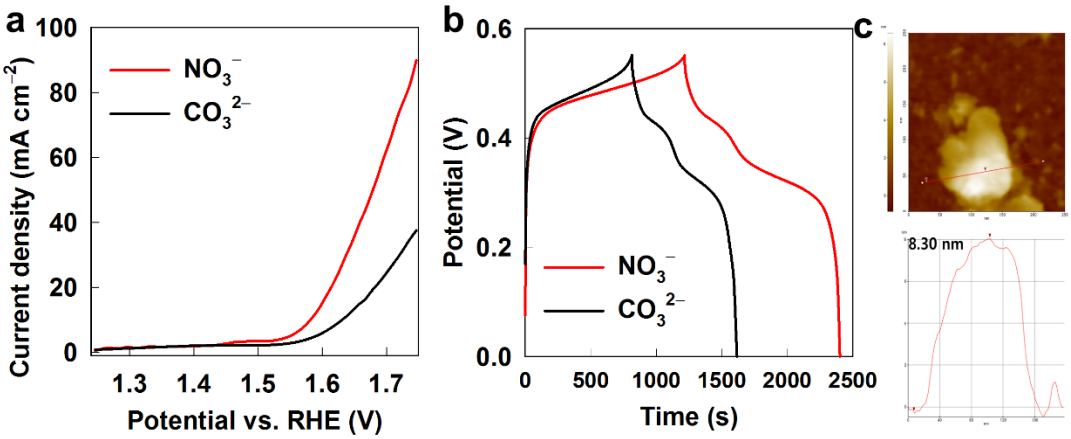


**Figure S16.** (a) LSV curves and (b) galvanostatic charge–discharge (CD) curves of Co–Al-LDH–$CO_3^{2-}$ and Co–Al-LDH–$NO_3^-$. (c) AFM image of the Co–Al-LDH–$CO_3^{2-}$.

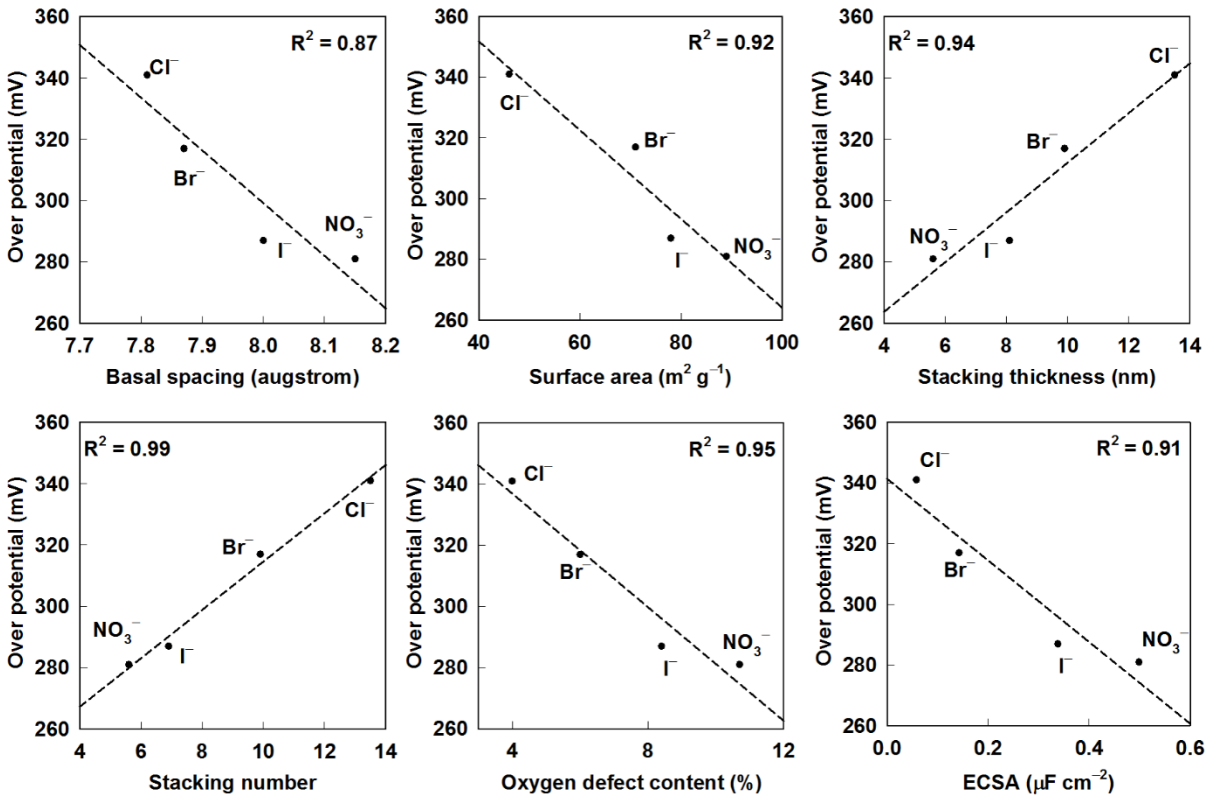


**Figure S17.** Correlation plots of overpotentials for restacked Co−Al-LDH NS as functions of basal spacing, surface area, stacking thickness, stacking number, oxygen defect content, and electrochemically active surface area (ECSA).

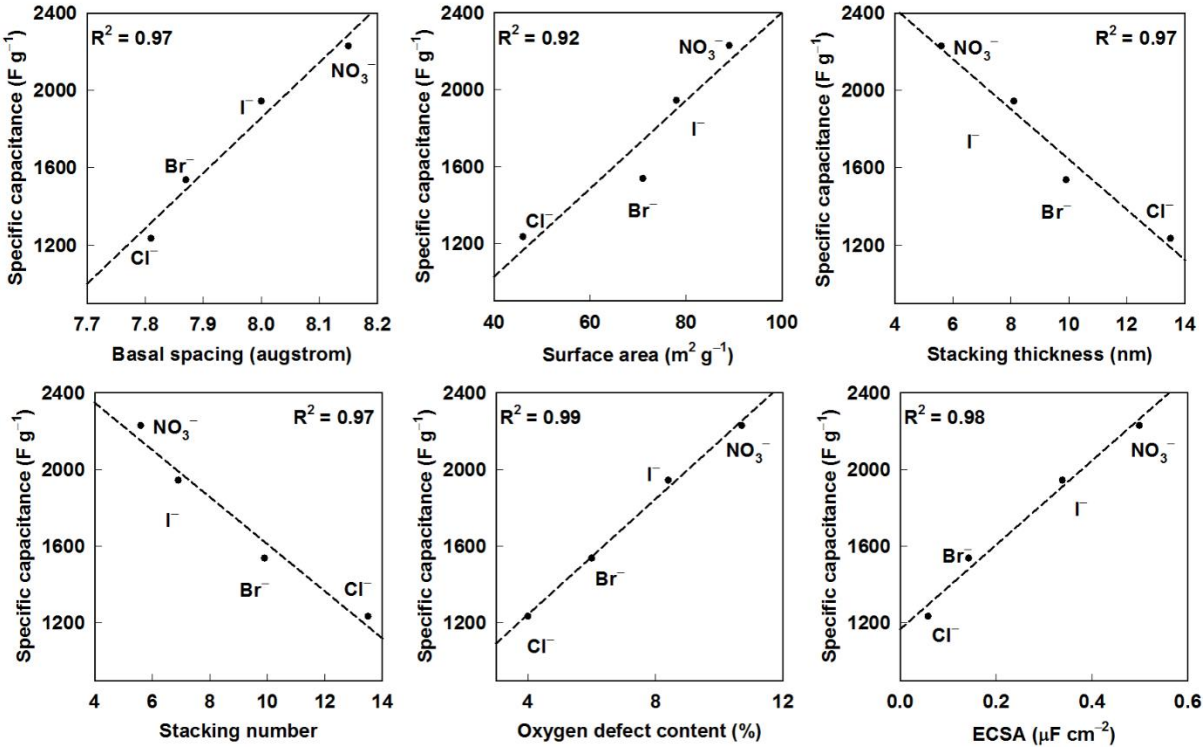


**Figure S18.** Correlation plots of specific capacitances for restacked Co–Al-LDH NSs as functions of basal spacing, surface area, stacking thickness, stacking number, oxygen defect content, and ECSA.

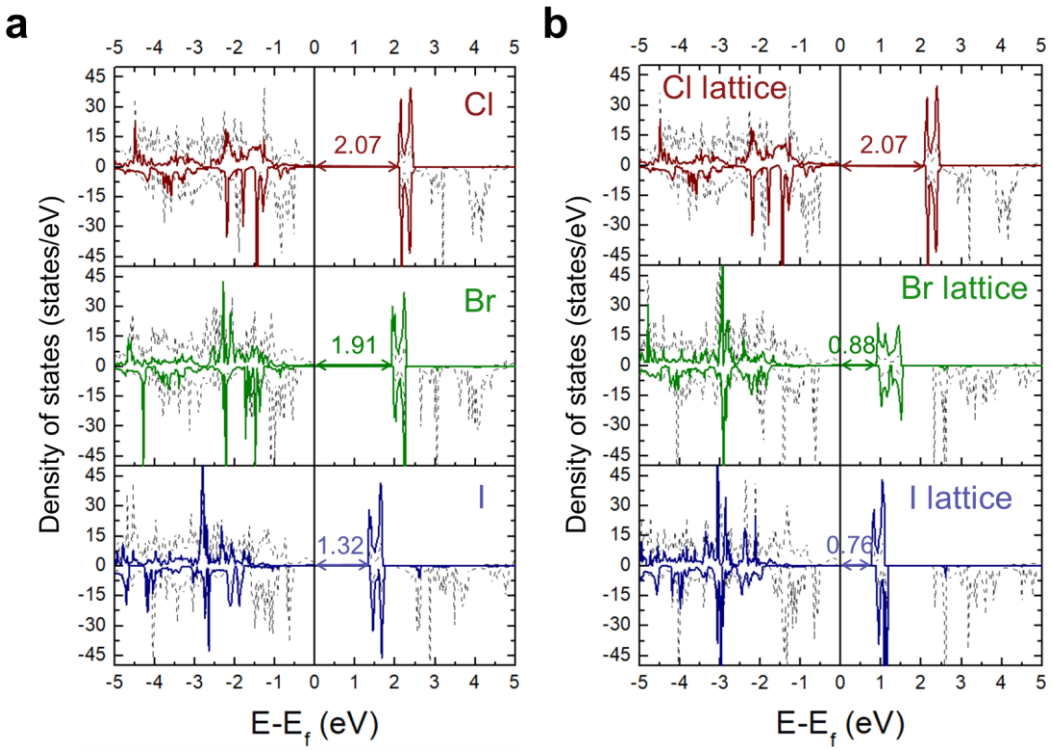


**Figure S19.** (a) Density of states (DOS) analyses for the model-2 consisting of $3Co^{2+}$–$1Al^{3+}$-LDH + $3Co^{2+}$–$1Co^{3+}$-LDH when the intercalant is $Cl^-$, $Br^-$, or $I^-$. Total DOS is shown using the black dashed line, and the partial DOS of the $Co^{3+}$ center is shown using the brown (Cl), green (Br), or blue (I) solid line, which is magnified by 5 times. (b) Total DOS and partial DOS of the $Co^{3+}$ are shown for the $Cl^-$-intercalated one (top), but with varying the c-lattice parameter to match it with the $Br^-$-intercalated one (middle) and the $I^-$-intercalated one (bottom).

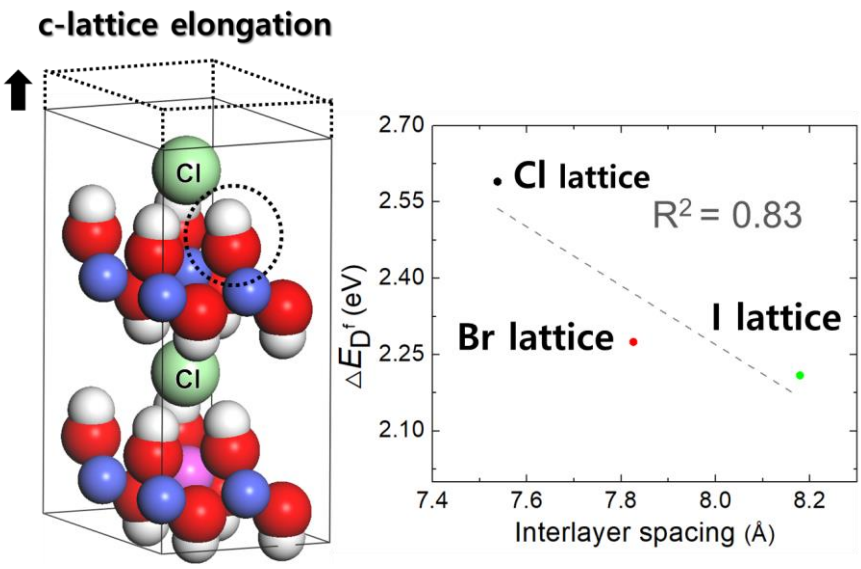


**Figure S20.** (a) Defect formation energies with only varying the c-lattice parameter for the model-2 consisting of $3Co^{2+}$–$1Al^{3+}$-LDH + $3Co^{2+}$–$1Co^{3+}$-LDH with an intercalant of $Cl^{-}$. The circled OH group is removed. The c-lattice parameter of the $Cl^{-}$-intercalated one (labeled as a "Cl lattice") is adjusted to match it with the $Br^{-}$-intercalated one (labeled as a "Br lattice") and the $I^{-}$-intercalated one (labeled as a "I lattice"). This is compared with the Figure 5b of the main manuscript.

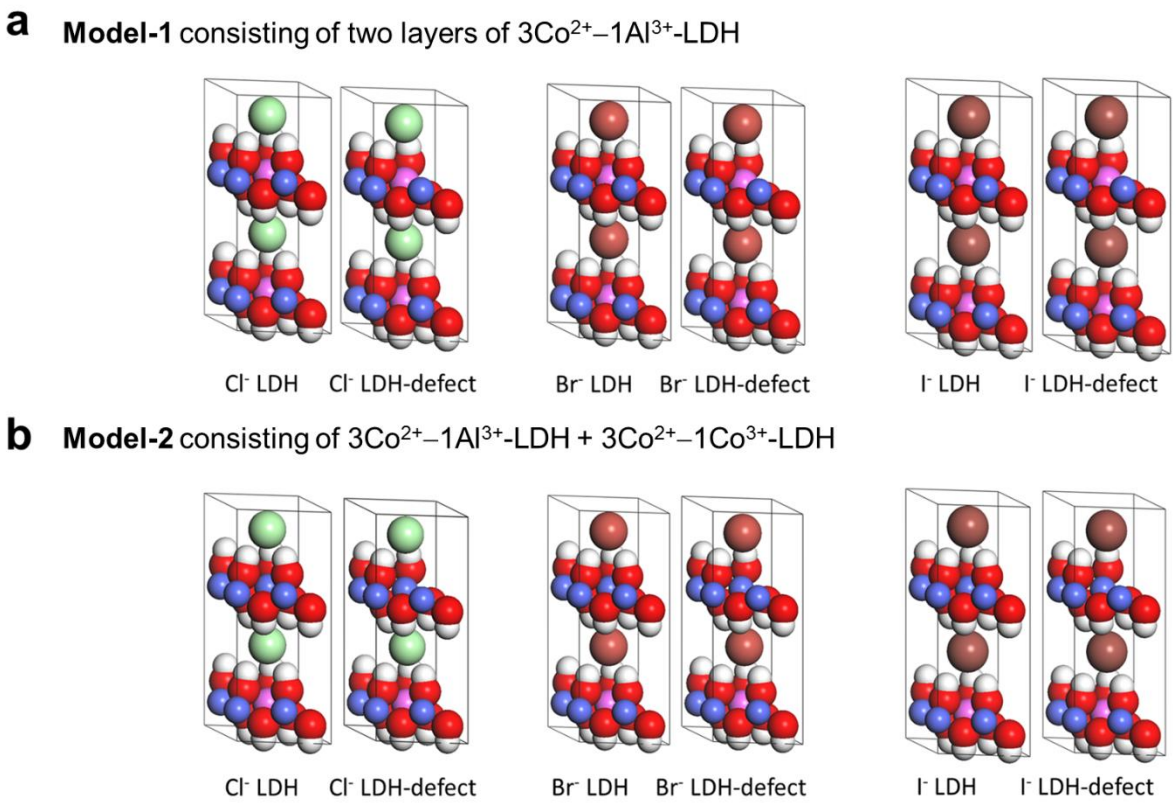


**Figure S21.** Density functional theory (DFT)-optimized structures of slab models for Co–Al-LDH systems ($3Co^{2+}$–$1Al^{3+}$-LDH + $3Co^{2+}$–$1Co^{3+}$-LDH). The structures of (a) model-1 and (b) model-2. Color codes for the structures are green for Cl, light brown for Br, deep brown for I, blue for Co, pink for Al, red for O, and white for H.

**Table S12.** DFT-optimized lattice parameters of model-1 LDH and model-2 LDH.

| **Model-1** | | | |
|---|---|---|---|
| Lattice parameters | $Cl^-$ | $Br^-$ | $I^-$ |
| a (Å) | 6.13 | 6.14 | 6.14 |
| b (Å) | 6.13 | 6.14 | 6.14 |
| c (Å) | 15.08 | 15.65 | 16.36 |
| **Model-2** | | | |
| Lattice parameters | $Cl^-$ | $Br^-$ | $I^-$ |
| a (Å) | 6.18 | 6.20 | 6.20 |
| b (Å) | 6.19 | 6.20 | 6.20 |
| c (Å) | 14.97 | 15.59 | 16.49 |

## REFERENCES


(1) Xiao, Y.; Su, D.; Wang, X.; Wu, S.; Zhou, L.; Fang, S.; Li, F. Layered Double Hydroxides with Larger Interlayer Distance for Enhanced Pseudocapacitance. *Sci. China Mater.* **2018**, *61*, 263–272.

(2) Li, H.; Musharavati, F.; Sun, J.; Jaber, F.; Zalnezhad, E.; Hui, K. N.; Hui, K. S. Investigation of the Electrochemical Properties of CoAl-Layered Double Hydroxide/$Ni(OH)_2$. *J. Electrochem. Soc.* **2018**, *165*, A407–A415.

(3) Liu, X.; Zhou, A.; Pan, T.; Dou, Y.; Shao, M.; Han, J.; Wei, M. Ultrahigh-Rate-Capability of a Layered Double Hydroxide Supercapacitor Based on a Self-Generated Electrolyte Reservoir. *J. Mater. Chem. A* **2016**, *4*, 8421–8427.

(4) Abushrenta, N.; Wu, X.; Wang, J.; Liu, J.; Sun, X. Hierarchical Co-Based Porous Layered Double Hydroxide Arrays Derived *via* Alkali Etching for High-Performance Supercapacitors. *Sci. Rep.* **2015**, *5*, 1–9.

(5) Han, S.; Chang, X.; Wu, D.; Chen, H.; Chen, D.; Liu, P.; Huang, T.; Jiang, X.; Huang, Q.; Lin, H. Hierarchically Porous Cobalt Aluminum Layered Double Hydroxide Flowers with Enhanced Capacitance Performances. *J. Mater. Sci.* **2017**, *52*, 6081–6092.

(6) Zai, J.; Liu, Y.; Li, X.; Ma, Z.; Qi, R.; Qian, X. 3D Hierarchical Co–Al Layered Double Hydroxides with Long-Term Stabilities and High Rate Performances in Supercapacitors. *Nano-Micro Lett.* **2017**, *9*, 1–9.

(7) Hong, W.; Wang, J.; Niu, L.; Sun, J.; Gong, P.; Yang, S. Controllable Synthesis of CoAl LDH@$Ni(OH)_2$ Nanosheet Arrays as Binder-Free Electrode for Supercapacitor Applications. *J. Alloys Compd.* **2014**, *608*, 297–303.

(8) Wang, S.; Huang, Z.; Li, R.; Zheng, X.; Lu, F.; He, T. Template-Assisted Synthesis of NiP@CoAl-LDH Nanotube Arrays with Superior Electrochemical Performance for

Supercapacitors. *Electrochim. Acta* **2016**, *204*, 160−168.